https://doi.org/10.5194/egusphere-2025-680
Preprint. Discussion started: 17 March 2025

All-Sky Temperature and Humidity Retrieval from the MWRI-RM Onboard the FY-3G Satellite

Minghua Liu[1], Wei Han[2, 3], Yunfan Yang[4, 5], Haofei Sun[4, 5], Ruoying Yin[2]

[1]School of Atmospheric Physics, Nanjing University of Information Science and Technology, Nanjing, 210044, China

[2]CMA Earth System Modeling and Prediction Centre (CEMC), China Meteorological Administration, Beijing, 100081, China

[3]State Key Laboratory of Severe Weather (LaSW), Chinese Academy of Meteorological Sciences, China Meteorological Administration, Beijing, 100081, China

[4]State Key Laboratory of Atmospheric Boundary Layer Physics and Atmospheric Chemistry (LAPC), Institute of Atmospheric Physics, Chinese Academy of Sciences, Beijing, 100029, China

[5]Institute of Atmospheric Physics, Chinese Academy of Sciences, Beijing, 100029, China

Correspondence to: Wei Han (hanwei@cma.gov.cn)

Abstract. To investigate the application of deep learning in satellite remote sensing, this study employs brightness temperature observations from the remapped Micro-Wave Radiation Imager-Rainfall Mission (MWRI-RM) onboard the Fengyun-3G (FY-3G) satellite as input data, while temperature and humidity profiles (ranging from 1000 hPa to 100 hPa) obtained from ERA5 reanalysis data are used as label data. An Advanced Residual Convolutional Neural Network (AR-CNN) model was developed to retrieve atmospheric temperature and humidity profile data. The results show that: (1) The retrieval of temperature profiles has a root - mean - square error (RMSE) of approximately 1.24 K, and the RMSE for humidity profile retrieval is 12.98%. (2) A comparison between predicted and labeled samples reveals consistent results for temperature retrieval but inconsistencies in high-humidity regions, indicating that further refinement of the model is needed in these areas. (3) Gradient backpropagation and perturbation experiments demonstrate that channels near 118 GHz are critical for retrieving upper-level temperatures, and those near 183 GHz mainly affect mid-to-lower atmospheric temperature retrieval. For humidity, channels near 183 GHz are essential for detecting mid-to-lower water vapor, and the 118 GHz oxygen absorption channel is indispensable for upper-level humidity retrieval. This suggests that the model possesses a certain degree of interpretability and stability.

https://doi.org/10.5194/egusphere-2025-680
Preprint. Discussion started: 17 March 2025

1. Introduction

In atmospheric science, temperature, relative humidity, and cloud liquid water content profiles are crucial for characterizing atmospheric thermodynamics and dynamics. Real-time global monitoring of these parameters is essential for weather forecasting, climate research, and meteorological support (Ebell et al., 2013; Liu et al., 2010; He et al., 2017). With continuous advancements in data assimilation and numerical weather prediction technologies, the quality requirements for meteorological data, including temperature and humidity measurements, have become increasingly stringent (Xu et al., 2024). Traditional data on temperature and humidity profiles are primarily obtained through radiosonde observations at meteorological stations. However, due to geographical constraints and other factors, these observational data exhibit low spatiotemporal resolution, increasingly failing to meet the stringent standards required for current operational needs and modern meteorological research (Yao et al., 2022). The rapid advancement of satellite remote sensing technology enables continuous and uniform observations of global atmospheric conditions. With high detection accuracy and broad coverage, it effectively addresses the significant deficiency of conventional data, such as atmospheric temperature and humidity profiles, in regions with sparse observational stations, including polar areas, oceans, and deserts (Rosenkranz et al., 2001). Because microwaves can penetrate clouds, haze, dust, and other atmospheric conditions, and are unaffected by solar radiation, microwave remote sensing offers unique advantages in spaceborne atmospheric remote sensing (Wang et al., 2010). This provides data with higher spatiotemporal resolution for retrieving atmospheric variables such as temperature and humidity, facilitating a more comprehensive and systematic understanding of the dynamic characteristics of the entire atmosphere and the material and energy exchanges between the upper and lower layers of the Earth's atmosphere (Zhu et al., 2001). Research on using satellite data to retrieve atmospheric parameter profiles has been ongoing for several decades. King (1958) was the first to propose deriving atmospheric temperature profiles based on satellite infrared emission radiation. With advancements in spaceborne detection technologies, significant progress has been made in the development of satellite remote sensing retrieval algorithms for atmospheric temperature and humidity profiles. Conventional retrieval algorithms can be broadly categorized into two types: statistical regression methods and physical retrieval methods. Statistical regression retrieval algorithms primarily involve using extensive datasets to establish a statistical regression model between radiance and the

https://doi.org/10.5194/egusphere-2025-680
Preprint. Discussion started: 17 March 2025

target atmospheric parameters (Cao et al., 2021), determining the optimal relationship between the two. The benefits of this approach include rapid computation and high solution stability. However, its simplicity does not account for the radiative transfer properties, and variations in sample characteristics can significantly affect retrieval accuracy. For instance, Smith (1970) developed an iterative method for retrieving atmospheric temperature and absorbing gas profiles using spectral and angular measurements of atmospheric radiation. In 1976, Smith et al. introduced a novel technique for retrieving atmospheric parameters from spectral radiation observations using the eigenvectors of the covariance matrix, referred to as the eigenvector regression retrieval method. Physical retrieval algorithms, in contrast, are based on the radiative transfer equation, deriving the target parameters from the measured spectral channel radiances of satellite instruments, grounded in robust physical principles. This method can more accurately represent atmospheric conditions, particularly in complex and variable atmospheric environments. However, physical retrieval methods also have certain drawbacks and limitations. First, because of the fundamental nature of the radiative transfer equation, pure physical retrieval methods have stringent requirements for weight functions (Cao et al., 2021) and are highly sensitive to observation errors, where small errors can lead to substantial deviations in retrieval results. Second, physical retrieval methods typically require substantial computational resources, and the solution process is relatively complex and time-consuming. Wu et al. (2005), using AIRS clear-sky observations, initially employed a statistical retrieval algorithm followed by a nonlinear physical retrieval algorithm to develop a physical retrieval algorithm for obtaining atmospheric temperature and humidity distributions. The results indicated that the root - mean - square error (RMSE) for near-surface atmospheric temperature retrieval was less than 1 K, and the RMSE for relative humidity retrieval was less than 10%. In recent years, the emergence of artificial intelligence technologies, particularly deep learning applications, has shown remarkable potential and broad prospects in the meteorological field, garnering significant attention from meteorological experts. Deep learning, an important branch of machine learning, excels at capturing high-level abstract representations from data and automatically extracting key features (Zhang et al., 2021; Xu et al., 2024). This capability makes deep learning particularly suitable and efficient for handling high-dimensional, nonlinear meteorological data. For example, Guan et al. (2010) used artificial neural network algorithms to retrieve the atmospheric vertical temperature profile under clear-sky conditions, based on real observation data from the infrared hyperspectral atmospheric sounder AIRS. The results showed that

https://doi.org/10.5194/egusphere-2025-680
Preprint. Discussion started: 17 March 2025

the artificial neural network algorithm could further enhance retrieval accuracy compared to the traditional eigenvector statistical method. Malmgren-Hansen et al. (2019) used convolutional neural networks (CNN) to retrieve atmospheric profiles from IASI sounding data. The results achieved higher accuracy than traditional statistical regression methods, illustrating that deep learning is a suitable method for atmospheric profile retrieval. Xu et al. (2024) proposed a method to retrieve atmospheric temperature profiles from FY-4A/GIIRS hyperspectral data using the TPE-MLP model. By incorporating additional parameters into the MLP and optimizing hyperparameters with TPE, a significant improvement in retrieval accuracy was achieved. Furthermore, factors affecting retrieval accuracy, including detector location, signal-to-noise ratio, terrain, solar altitude angle, and satellite zenith angle, were analyzed. The results showed monthly and diurnal variations and compared favorably with ERA5 and in situ sounding data, with mean biases ranging from -0.56 K to 0.60 K and standard deviations from 1.26 K to 2.17 K, demonstrating the effectiveness of the proposed model. On April 16, 2023, China successfully launched its first precipitation measurement satellite, FY-3G (also known as the Precipitation Satellite), equipped with an upgraded version of the Micro-Wave Radiation Imager-Rainfall Mission (MWRI-RM) from the FY-3B series. This upgrade integrates imaging and sounding functions through a unified design (Gu et al., 2023), adding temperature sounding channels near the oxygen absorption bands at 54 GHz and 118 GHz, and humidity sounding channels near the water vapor absorption band at 183 GHz. With a total of 26 sounding channels, it significantly improves the capability and performance metrics for detecting precipitation and profiling atmospheric temperature and humidity (Zhang et al., 2023). Leveraging neural network algorithms enables the fitting of complex nonlinear equations, providing robust computational power without requiring an in-depth analysis of the nonlinear mappings themselves (Cadeddu et al., 2009; Cai et al., 2020; Cao et al., 2021). Using MWRI-RM sounding data, this study employs an Advanced Residual Convolutional Neural Network (AR-CNN) to retrieve atmospheric temperature and relative humidity profiles. To further enhance the study's objectives, we aim to analyze the model's interpretability, which is crucial for understanding the decision-making process and increasing trust in deep learning-based methods. Additionally, the significance of the 118 GHz and 183 GHz channels in retrieving temperature and relative humidity profiles will be emphasized. These specific frequency bands are essential for accurately capturing atmospheric water vapor and temperature, as they are sensitive to the absorption characteristics of water vapor, making them critical for precise inversion of vertical profiles in weather

https://doi.org/10.5194/egusphere-2025-680
Preprint. Discussion started: 17 March 2025

prediction and climate modeling. By integrating these considerations, the research aims to enhance both the performance and transparency of deep learning applications in atmospheric science, providing improved data-driven insights for numerical weather prediction.

2. Data

2.1 Instrument Overview

The primary purpose of the MWRI-RM is to collect microwave radiation data from both land and sea surfaces globally, serving the needs of global precipitation measurement. It employs a conical scanning system, featuring 1648 scan lines with 492 sampling points on each line. The MWRI-RM is equipped with 8 feed sources arranged in two rows. The first row consists of channels at 10 GHz, 18.7 GHz, 23.8 GHz, 36 GHz, and 89 GHz, where the 18.7 GHz and 23.8 GHz channels share a common feed source. The second row comprises channels at 54 GHz, 118 GHz, 166 GHz, and 183 GHz. The feed sources in different rows have angular differences in their observation geometries. The MWRI-RM functions across 17 frequency points, encompassing 26 channels, with certain frequencies featuring dual-polarization capabilities. Detailed channel specifications are delineated in Table. 1.

Table 1: Channel information of FY-3G/MWRI-RM (data source: FY-3G_L1 Data User's Guide_MWRI-RM_20230625.pdf (nsmc.org.cn))

Center Frequency (GHz)	Polarization Mode	Bandwidth (MHz)	Frequency Stability (MHZ)	IFOV (km×km)	Main Applications
10.65	V,H	180	10	21×35	Intense precipitation over the ocean, land surface products.
18.7	V,H	200	10	14×23	Precipitation over the ocean, land surface products.
23.8	V,H	400	15	13×21	Total water vapor over oceans.
36.5	V,H	900	20	9×15	Precipitation, land surface products.
50.30	V,H	400	25	7×11	Precipitation, drizzle,
52.61	V,H	400	25	7×11	Snowfall, height and
53.24	V,H	400	25	7×11	thickness of the melting
53.75	V,H	400	25	7×11	layer.
89.0	V,H	3000	25	5×8	Precipitation and

https://doi.org/10.5194/egusphere-2025-680
Preprint. Discussion started: 17 March 2025

					snowfallover ocean and land areas, land surface products.
118.7503±3.2	V	2x500	25	4×7	
118.7503±2.1	V	2x400	25	4×7	Precipitation, drizzle, Snowfall, height and thickness of the melting layer.
118.7503±1.4	V	2x400	25	4×7	
118.7503±1.2	V	2x400	25	4×7	
165.5±0.75	V	2x1350	30	4×6	Precipitation and snowfall overland.
183.31±2.0	V	2x1500	30	4×7	
183.31±3.4	V	2x1500	30	4×7	Snowfall, cloud ice.
183.31±7	V	2x2000	30	4×7	

2.2 Sample Construction

This study utilizes MWRI-RM L1 products from October 23 to November 23, 2023 (UTC), comprising sea surface brightness temperatures derived from raw L1 data and preprocessed static parameters through decoding and quality checks. Sea data were exclusively selected to minimize training costs. After remapping using an enhanced BGI algorithm that aligns spatial resolutions and footprint centers (Chen et al., 2024), all channels were resampled to the 23.8 GHz channel's resolution of 13 km×21 km. ERA5 reanalysis data(Hersbach et al., 2023), featuring global temperature profiles across 27 levels (1000 hPa to 100 hPa) at 0.25°× 0.25°spatial resolution, were selected as labels for the satellite data. Given the resolution discrepancies, ERA5 temperature profiles were interpolated to match MWRI-RM observation points. Observation times were rounded to the nearest hour, and ERA5 data were selected and interpolated using a nearest-neighbor approach based on satellite data coordinates. The data were formatted into a (samples, height, width, channels) structure: 13,100,161 samples, each 5×5 in size, with 26 channels. Corresponding ERA5 temperature and humidity profiles at the center of each sample were used as labels, as depicted in Fig. 1. Samples were chronologically ordered, with 80%(10,480,128 samples) for training, 20%(2,620,032 samples) for testing, and 20%(2,096,025 samples) of the training set randomly selected for validation, completing the data preparation for the neural network model.

https://doi.org/10.5194/egusphere-2025-680
Preprint. Discussion started: 17 March 2025

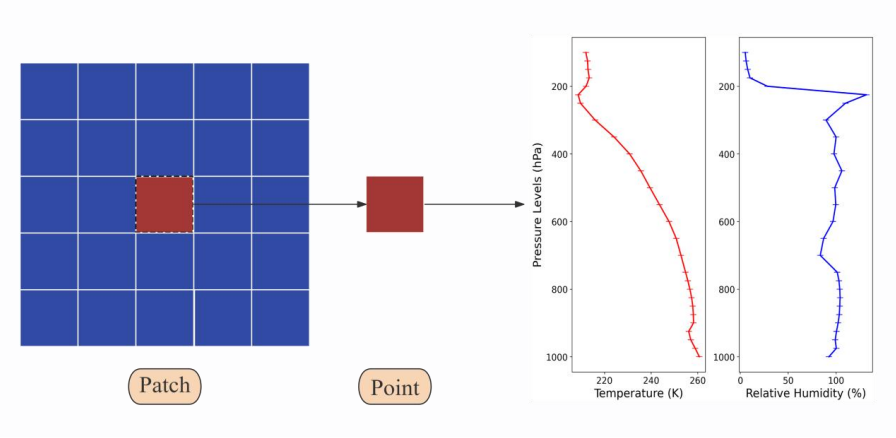

Figure 1: Illustration of retrieval from area to point

3 Retrieval Methods

3.1 AR-CNN Network Algorithm Principles

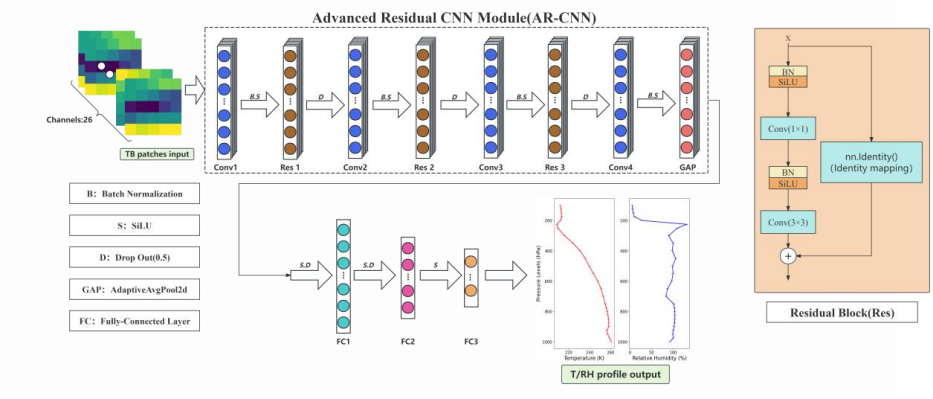

Figure 2: Network architecture for Advanced Residual CNN (AR-CNN)

In this study, an Advanced Residual Convolutional Neural Network (AR-CNN) was developed to retrieve temperature and humidity profiles (Fig. 2). The network architecture integrates convolutional layers, residual blocks, batch normalization, dropout, adaptive average pooling, and fully connected layers to efficiently extract features from 5×5 satellite brightness temperature images with 26 channels. SiLU activation, known for its smooth gradient properties and ability to avoid dead zones, is employed throughout the network (Elfwing et al., 2018). Residual blocks, equipped with skip connections, mitigate gradient vanishing in deep layers (He et al., 2016). A dropout layer with a rate of 0.25 is incorporated to prevent overfitting. The final convolutional layer generates a 512-channel feature map,

https://doi.org/10.5194/egusphere-2025-680
Preprint. Discussion started: 17 March 2025

which is normalized and compressed via adaptive average pooling to 1×1 per channel. The fully connected layers predict temperature and humidity profiles across 27 layers. An early stopping mechanism is implemented during training to enhance model generalization. The AR-CNN's design effectively captures multi-level features and improves training efficiency and generalization, making it well-suited for complex image classification tasks.

3.2 Retrieval Algorithm Validation

In this paper, bias and root - mean - squared error (RMSE) are chosen as evaluation metrics for the accuracy of atmospheric temperature and relative humidity profile retrieval. The specific formulas are as follows:

$$\text{Bias} = \frac{1}{N}\sum_{i=1}^{Ns}(x_i - y_i) \quad (1)$$

Where is the xi retrieved value, yi is the target value, and N is the number of samples.

Bias evaluates the systematic error of the model, representing the average difference between the predicted and true values. A bias of zero indicates no systematic deviation, while a positive or negative bias indicates that the model tends to overestimate or underestimate the target variable, respectively.

$$\text{RMSE} = \sqrt{\frac{1}{N}\sum_{i=1}^{Ns}(x_i - y_i)^2} \quad (2)$$

Where xi is the retrieved value, yi is the target value, and N is the number of samples.

RMSE assesses the magnitude of errors between predicted and true values. It is sensitive to large errors due to the squaring of the differences. A lower RMSE indicates better model performance, with smaller deviations between the retrieved and target values.

4. Results

4.1 Temperature Retrieval

The model evinces a relatively uniform distribution of bias (0.11 K) and RMSE (1.24 K) across diverse atmospheric layers, as depicted in Fig. 3(a)-(b), manifesting overall consistency in its performance. Nevertheless, the layer - dependent variations in RMSE imply that there exist areas where the model might not comprehensively account for the intricate complexities of the atmosphere. Notably, the RMSE is relatively more pronounced in the lower troposphere around 850 hPa. This is likely

https://doi.org/10.5194/egusphere-2025-680
Preprint. Discussion started: 17 March 2025

attributable to the substantial surface influences, especially those stemming from the variability of sea surface temperature (SST). Such variability engenders complexity in the retrieval of temperature near the Earth's surface (Susskind et al., 2003). The non - linear interactions between the surface and the atmosphere, in conjunction with the sensor's sensitivity to the lower atmospheric layers, might not have been adequately learned by the model.

With the progressive increase in altitude from 850 hPa to 500 hPa, the RMSE gradually dwindles, reaching a minimum value of approximately 1 K at 500 hPa. This decrease can be ascribed to the relatively stable and homogeneous temperature field within the mid - troposphere, where the vertical mixing is less conspicuous compared with that in the lower and upper troposphere. Within this region, the model derives advantages from more consistent radiometric data, resulting in more accurate predictions.

Above 500 hPa, the RMSE commences to increase once more, reaching its zenith around 100 hPa. This increase is ascribed to the complex dynamics in the upper troposphere and the lower stratosphere, involving intense vertical motion, convective processes, along with the phase transitions of water vapor, clouds, and ice particles (Chen et al., 2003; Susskind et al., 2003). Furthermore, the sensitivity of the instrument declines at higher altitudes on the grounds of the reduced radiative energy emission and the limited sensitivity of the sensor in these regions (Sahoo et al., 2015), giving rise to lower signal - to - noise ratios and less informative data for temperature inversion.

Fig. 3(c)-(h) further validate these findings. The histogram presented in Fig. 4, which compares the counts of inversion samples with those of labeled samples, discloses the difficulties in accurately retrieving extremely high and low temperatures. This challenge is prevalent in satellite remote sensing, especially in the retrieval of microwave channels, and might originate from data imbalance, in which extreme temperatures are inadequately represented in training datasets. Consequently, the model may exhibit a proclivity towards more common temperature ranges, thereby undermining its performance on extreme values. Moreover, complex meteorological interactions, such as those related to moisture content, pressure systems, and radiative transfer processes, might not be comprehensively captured by the input features of the model (Wang et al., 2023). The inherent variability and non - linearity of atmospheric processes, particularly during extreme weather events, introduce further complexity, thereby exacerbating the retrieval inaccuracies in the context of microwave channel data (Wang et al., 2021).

https://doi.org/10.5194/egusphere-2025-680
Preprint. Discussion started: 17 March 2025

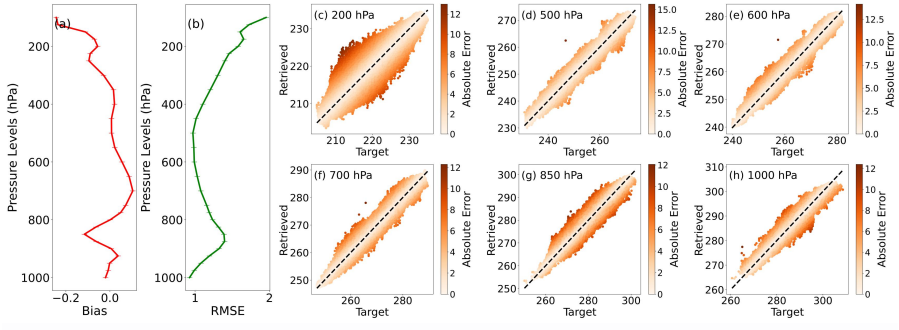

Figure 3: (a)-(b) Bias and RMSE of the retrieved temperature profile; (c)-(h) Scatter plot of the retrieved temperature at specific pressure levels (Lighter colors indicate smaller errors) (c)200hPa; (d)500hPa; (e)600Pa; (f)700hPa; (g)850hPa; (h)1000hPa

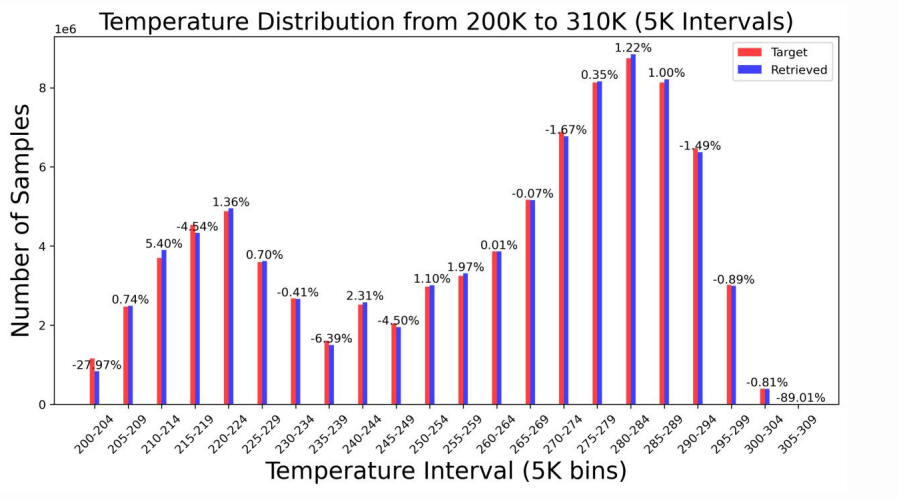

Figure 4: Statistics of the number of retrieved and labeled samples in the test set (5K bins)

The analysis of the Jacobians for temperature and relative humidity, which were obtained using the Radiative Transfer for TOVS (RTTOV) model customized for the MWRI-RM sensor, was carried out by means of gradient backpropagation to evaluate the contributions of individual input channels. (The weights of model.conv1 are extracted, the importance of each input channel is computed by summing the absolute weights across all output channels and spatial dimensions, and these values are normalized for comparison). The results suggest that the highest weight in the retrieval of the temperature profile resides within the 118.7503±1.2 GHz frequency band (Fig. 5(a)), being in consonance with the peak sensitivity of the temperature Jacobians (Fig. 5(b)). This observation is remarkable, as it highlights the model's aptitude for utilizing the oxygen absorption line near 118 GHz, a crucial spectral signature that

https://doi.org/10.5194/egusphere-2025-680
Preprint. Discussion started: 17 March 2025

affords significant sensitivity to temperature fluctuations in the atmosphere. This specific line is acknowledged for its high responsiveness to temperature changes in the upper - to - mid - troposphere, where the rotational transitions of oxygen predominantly govern the radiative transfer processes (Gasiewski et al., 1989, 1993). Moreover, the 183.31 ± 7 GHz channel, which is related to the water vapor absorption band, plays an equally vital role in the retrieval of the temperature profile. This channel is of great significance because the absorption features of water vapor within this frequency range affect the radiance measured by the sensor, thus furnishing valuable information for temperature retrieval (Yao et al., 2022). Water vapor, as a highly variable atmospheric constituent, affects the atmospheric radiation via its absorption and emission processes. Therefore, the 183.31±7 GHz channel, which is sensitive to water vapor variations, contributes to the refinement of the temperature profile retrieval, particularly in regions where the water vapor content is substantial and its influence on the radiative budget is prominent.

In order to evaluate the stability of our model in the face of observational errors and to enhance its physical interpretability, we perturbed the brightness temperatures of the 118.7503 ± 1.2 GHz and 183.31 ± 7 GHz channels (Fig. 6). This analysis discloses that the 118.7503 ± 1.2 GHz channel principally affects the temperature retrievals in the upper troposphere, whereas the 183.31 ± 7 GHz channel is more sensitive to the temperatures in the mid - to - lower troposphere. These findings are in accordance with the temperature Jacobians, which demonstrate distinct vertical sensitivities for each channel. The 118 GHz channel interacts with the atmospheric layers characterized by robust oxygen absorption, while the 183 GHz channel is more sensitive to water vapor, which is more abundant in the lower and mid - troposphere, thus contributing to a more region - specific temperature signature (He et al., 2017).

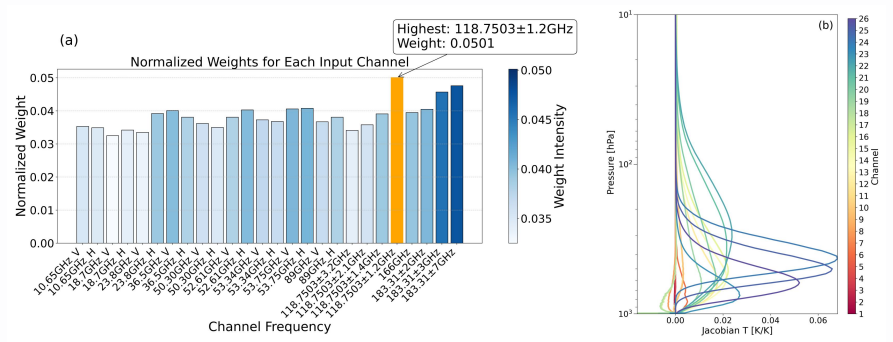

https://doi.org/10.5194/egusphere-2025-680
Preprint. Discussion started: 17 March 2025

Figure 5: (a) Weighting map for temperature profile retrieval channels; (b) Jacobian for temperature, obtained using the RTTOV model tailored for the MWRI-RM sensor

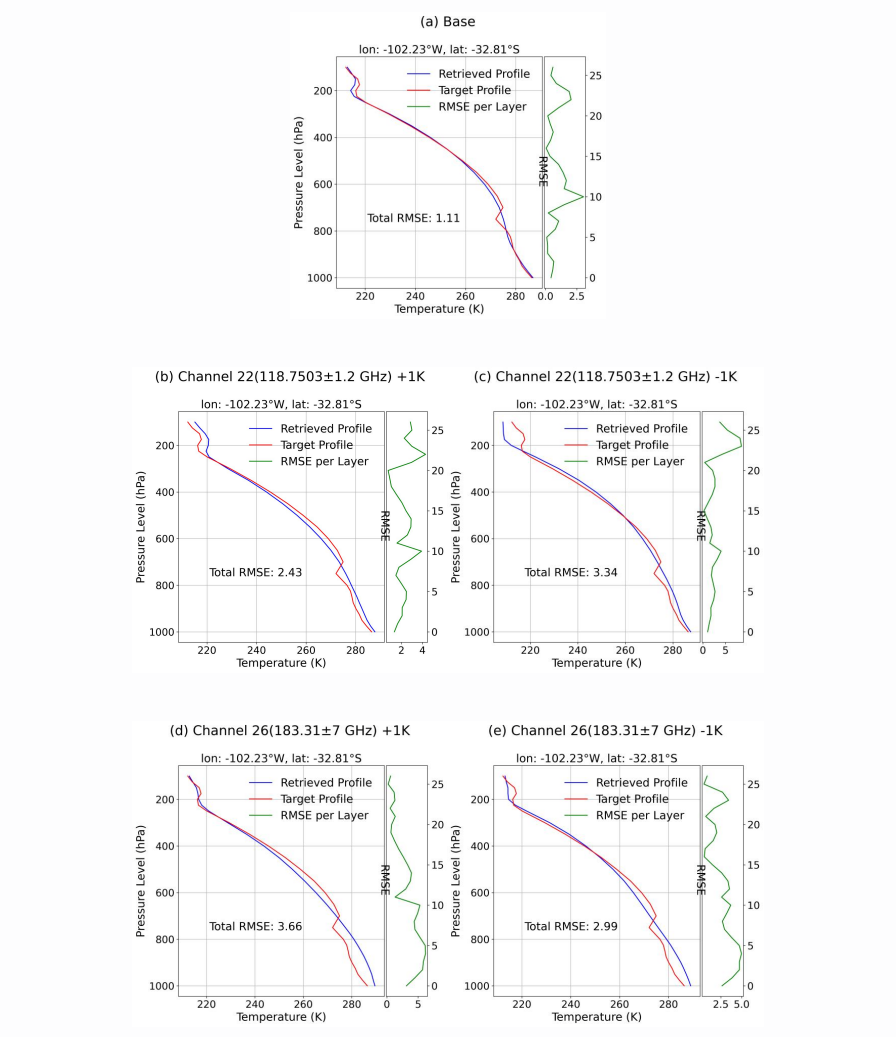

Figure 6: Single temperature profile perturbation experiment (introducing ±1K perturbations to the brightness temperatures of channels 22 and 26)

4.2 Relative Humidity(RH) Retrieval

Across various atmospheric layers, the model demonstrated a relatively consistent performance, presenting a bias of 0.87% and a RMSE of 12.98%, as graphically depicted in Fig. 7(a)-(b). The consistent performance indicates the model's general stability in handling different atmospheric

https://doi.org/10.5194/egusphere-2025-680
Preprint. Discussion started: 17 March 2025

conditions, yet the non - zero bias and RMSE values also suggest room for improvement in its accuracy.

Nevertheless, remarkable variations in RMSE were discerned, especially in the lower troposphere at approximately 900 hPa. These variations can be mainly ascribed to the surface heterogeneity, which encompasses diverse land - cover types and their associated surface - atmosphere interactions, and the complex humidity gradients in the vicinity of the Earth's surface. Such factors introduce additional complexity to the humidity retrieval process, making it more challenging for the model to accurately capture the true humidity values in these regions. In oceanic regions, SST and surface fluxes play a pivotal role in introducing significant variability. The dynamic nature of SST, influenced by ocean currents, solar radiation, and heat exchange processes, and the complex surface fluxes, including latent and sensible heat fluxes, disrupt the straightforward relationship between brightness temperature variations and humidity fluctuations. This disruption consequently impedes the model's accuracy in accurately retrieving humidity values in these near - surface layers, highlighting the need for more refined models or additional data sources to account for these complex ocean - atmosphere interactions.

With the progressive increase in altitude commencing from 800 hPa and ascending, the RMSE experiences a gradual escalation, reaching its peak value at around 200 hPa. This upward trend in RMSE indicates a growing complexity in the humidity retrieval process as the altitude increases, potentially due to the increasing influence of dynamic and turbulent processes in the mid - to - upper troposphere. This trend can be principally ascribed to the dynamic and turbulent characteristics inherent in the mid - to - upper troposphere. In this altitude range, convective processes, which involve the vertical transport of heat and moisture, and cloud - related processes, such as the formation, growth, and phase changes of cloud particles, introduce substantial uncertainty. These complex meteorological processes not only affect the radiative transfer of microwave signals but also alter the local humidity distribution, making it difficult for the model to accurately retrieve humidity values based solely on the observed brightness temperatures (Burns et al., 1995, 1997; Blackwell et al., 2005; Zhang et al., 2021).

These complex meteorological processes, especially in regions of deep convection or in the presence of liquid water droplets and ice crystals, obfuscate the direct correlation between radiometric observations and humidity. The strong absorption and scattering of microwave signals by these hydrometeors disrupt the information - carrying capacity of the radiometric data, thereby diminishing the model's

https://doi.org/10.5194/egusphere-2025-680
Preprint. Discussion started: 17 March 2025

sensitivity to water vapor changes. This reduction in sensitivity ultimately leads to less accurate humidity retrievals in these complex atmospheric conditions (Wang et al., 2010; Tan et al., 2015).

Fig. 7(c)-(h) further validate these findings. However, the wider scatter distribution in the relative humidity retrieval results, as depicted in these figures, clearly indicates a lower level of precision. This broader scatter could be attributed to a combination of factors, such as the complex nature of humidity - related processes, uncertainties in the input data, and limitations in the model's ability to capture all relevant physical mechanisms governing humidity variations. Fig. 8 illustrates the suboptimal retrieval performance in low - humidity regions at low latitudes and high - humidity regions at high latitudes. This graphical representation clearly highlights the difficulties encountered in accurately retrieving extremely high and low relative humidity values. Similar to the challenges faced in temperature profile retrieval, the issues in humidity retrieval can be traced back to data - related problems, such as data imbalance in the training dataset, and the complex non - linear relationships between the input variables and the humidity values in extreme conditions.

The challenges encountered in retrieving extreme relative humidity values can be ascribed to multiple interrelated factors. First and foremost, the rarity of extreme humidity events results in a significant data imbalance in the training datasets. In such imbalanced datasets, the model tends to be biased towards the more frequently occurring common humidity ranges during the training process. This bias ultimately leads to suboptimal performance when the model is applied to extreme humidity conditions, as it lacks sufficient exposure to the unique characteristics and patterns associated with extreme humidity events. Moreover, humidity retrieval via microwave channels is significantly affected by surface emissivity, the variable distribution of atmospheric water vapor, and the presence and characteristics of cloud cover. These factors interact in complex ways, introducing substantial complexity and uncertainty into the retrieval process. For example, surface emissivity can vary greatly depending on the underlying surface type, and cloud cover can either absorb or scatter microwave signals, both of which can distort the relationship between the observed brightness temperatures and the actual humidity values (Tan et al., 2015). The existence of clouds substantially impacts microwave signals, thereby complicating the humidity retrieval process from satellite - based data. Clouds, especially those with high liquid water content or ice crystal concentrations, can strongly absorb and scatter microwave radiation. This absorption and scattering not only attenuate the signal strength but also modify the spectral characteristics of the received signals, making it extremely challenging to

https://doi.org/10.5194/egusphere-2025-680
Preprint. Discussion started: 17 March 2025

accurately extract humidity - related information from the satellite - observed brightness temperatures (Yao et al., 2022).

In contrast to temperature retrieval, which is relatively less influenced by these factors, humidity retrieval confronts more formidable challenges. The vulnerability of microwave signals to attenuation and scattering by various atmospheric constituents, such as water vapor, clouds, and aerosols, is a major contributing factor. In extreme humidity conditions, the high concentration of water vapor and the possible presence of extensive cloud cover can exacerbate these effects, leading to a significant degradation in the signal - to - noise ratio. As a result, the errors in humidity retrieval increase substantially, highlighting the need for more advanced retrieval algorithms and data - correction techniques to mitigate these issues (He et al., 2017).

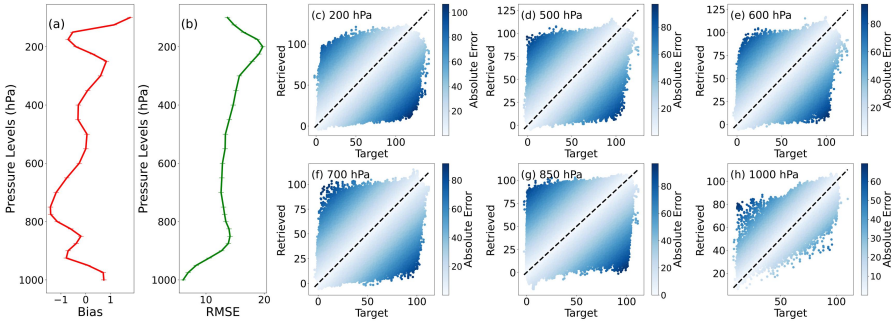

Figure 7: (a)-(b) Bias and RMSE of the retrieved RH profile; (c)-(h)Scatter plot of the retrieved RH profile at specific pressure levels (Lighter colors indicate smallererrors) (c)200hPa; (d)500hPa; (e)600Pa; (f)700hPa; (g)850hPa; (h)1000hPa

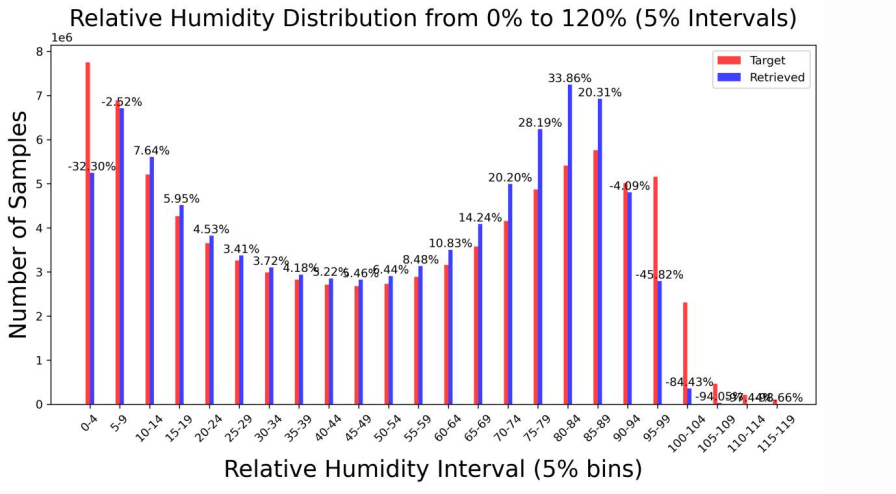

Figure 8: Statistics of the number of retrieved and labeled samples in the test set (5% bins)

https://doi.org/10.5194/egusphere-2025-680
Preprint. Discussion started: 17 March 2025

By means of gradient - based backpropagation analysis, we investigate the learned weights of the input channels. It becomes apparent that the most significant weights for retrieving the atmospheric humidity profile are predominantly concentrated around the 183.31 ± 7 GHz channel (Fig. 9(a)), which corresponds precisely to the water vapor absorption line near 183.31 GHz. This spectral characteristic is of critical importance because it aligns closely with the peak sensitivity of the humidity Jacobians (Fig. 9(b)). This alignment strongly indicates that the model has successfully learned that this frequency range offers crucial information for retrieving the vertical distribution of water vapor in the atmosphere.

Furthermore, the 118.7503 ± 1.2 GHz channel assumes a vital role in the retrieval of the humidity profile, especially in the upper troposphere and lower stratosphere. Perturbation experiments (Fig. 10) carried out on the brightness temperatures at both 183.31±7 GHz and 118.7503±1.2 GHz frequencies yield results similar to those observed in temperature sensitivity studies. Specifically, the 183.31 ± 7 GHz channel principally affects the retrieval of mid - to - lower level humidity, whereas the 118.7503± 1.2 GHz channel displays a higher sensitivity to higher altitude humidity, especially in the upper troposphere. These findings are in close accordance with the characteristics of the humidity Jacobians (Fig. 9(b)), strengthening the model's ability to capture the distinct vertical layers of moisture in the atmosphere.

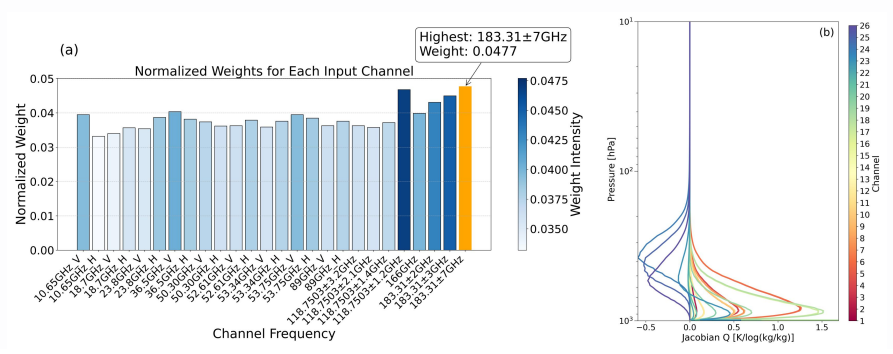

Figure 9: (a) Weighting map for RH profile retrieval channels; (b) Jacobian for relative humidity, obtained using the RTTOV model tailored for the MWRI-RM sensor

https://doi.org/10.5194/egusphere-2025-680
Preprint. Discussion started: 17 March 2025

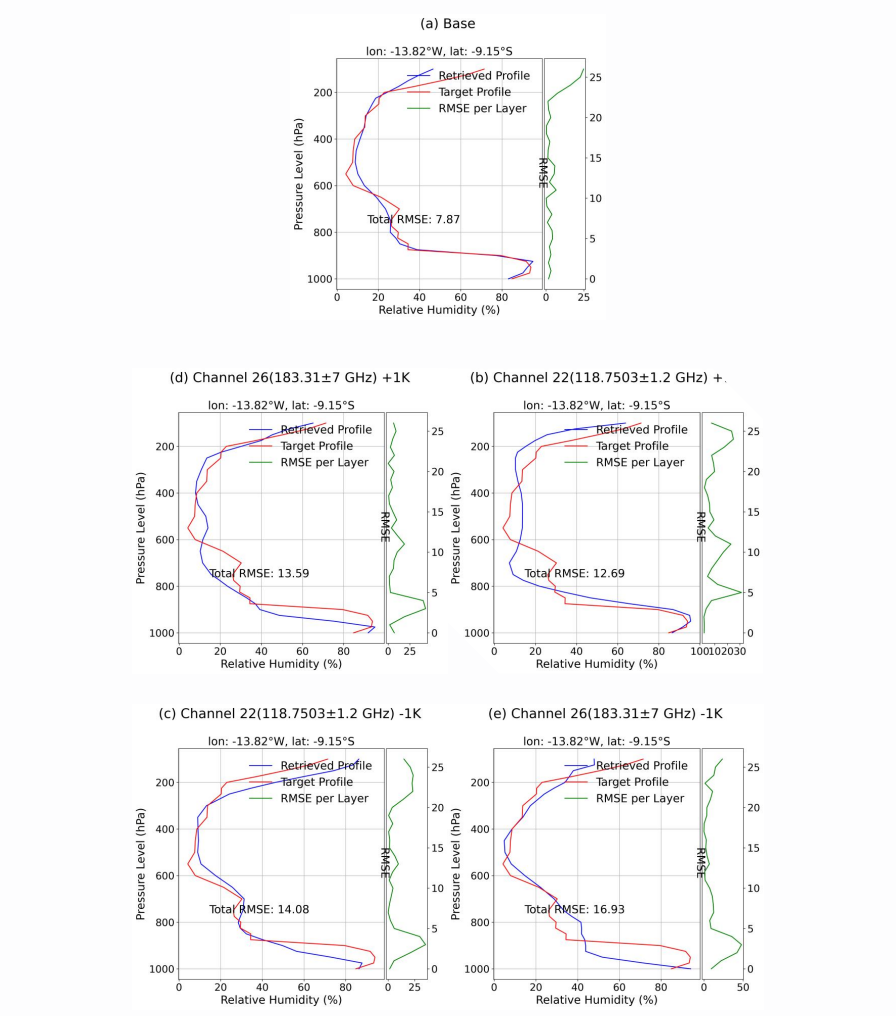

Figure 10: Single RH profile perturbation experiment (introducing ± 1K perturbations to the brightness temperatures of channels 22 and 26)

5. Conclusions

This study employs remapped MWRI-RM sea - surface - observed brightness temperature data, with ERA5 reanalysis temperature and humidity profile sets functioning as label data, to retrieve temperature and humidity profiles by means of an Advanced Residual Convolutional Neural Network (AR - CNN). The findings can be summarized as follows:

The retrieval of temperature profiles exhibits a root - mean - square error (RMSE) of approximately 1.24 K, while the RMSE for the humidity profile retrieval is 12.98%. These values demonstrate a high

https://doi.org/10.5194/egusphere-2025-680
Preprint. Discussion started: 17 March 2025

level of accuracy in both temperature and humidity profile retrieval, indicating the effective performance of the model in capturing atmospheric variables accurately.

A statistical comparison of the number of prediction samples vis - à - vis label samples unveils that for temperature profile retrieval, the counts are generally consistent, manifesting the model's robust ability to perform across a wide range of temperature conditions. However, discrepancies were detected in the number of prediction and label samples in high - humidity regions. This implies that the model's performance in retrieving humidity profiles in high - humidity environments may be less accurate, potentially attributable to the inherent challenges in determining water vapor content in such regions. Consequently, further refinement of the model may be necessary to achieve optimal performance in these conditions.

A comprehensive analysis incorporating the instrument's channel weight functions with Jacobian matrices for temperature and relative humidity uncovered a strong alignment achieved through gradient backpropagation, validating the rationality of the model's utilization of channel information. Channels near 118 GHz were crucial for retrieving upper - level temperature and humidity, while those near 183 GHz principally contributed to mid - to - lower atmospheric profiles, in accordance with their expected vertical sensitivities. Perturbation experiments conducted on the critical channels (118.7503 ± 1.2 GHz and 183.31 ± 7 GHz) verified their significant contributions and exhibited the model's stability and interpretability.

Appendix A.

https://doi.org/10.5194/egusphere-2025-680
Preprint. Discussion started: 17 March 2025

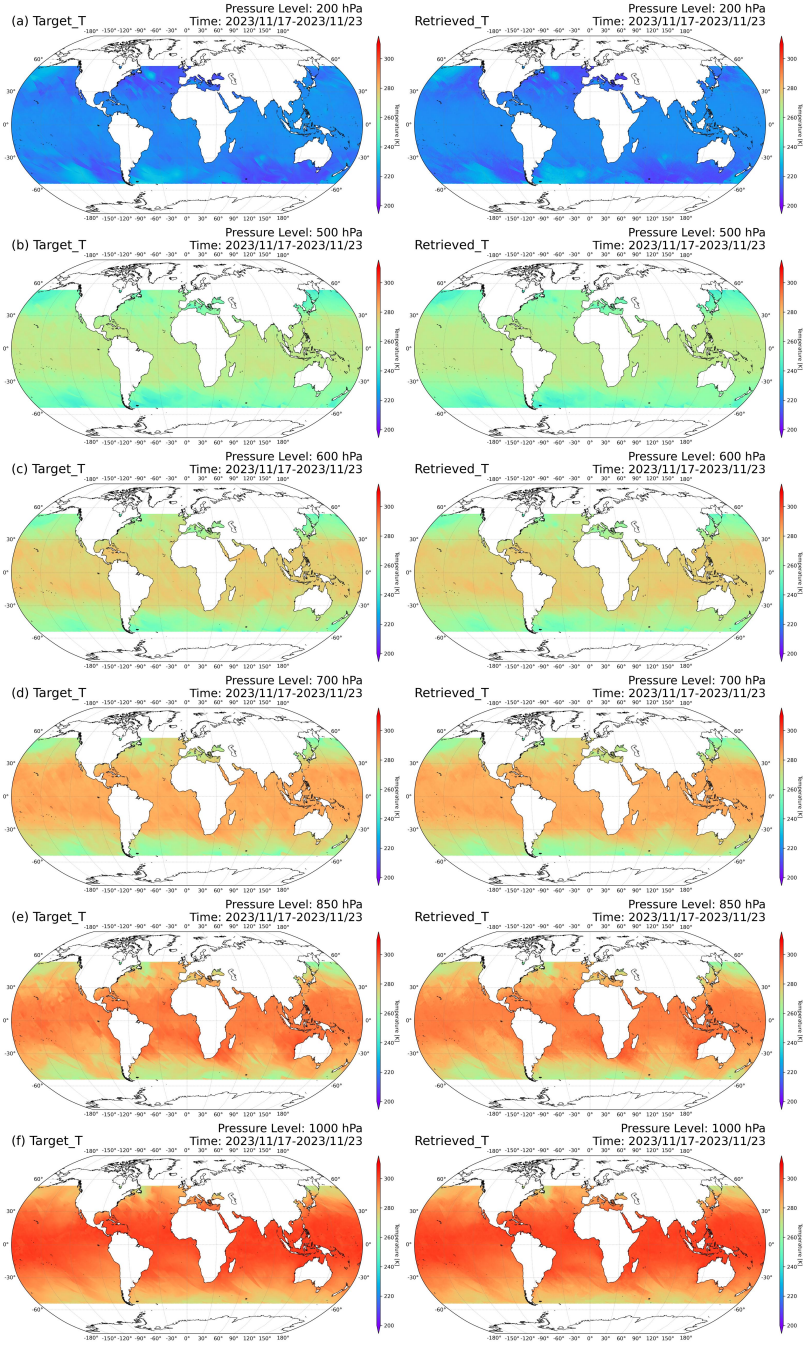

Fig. A1: Global Comparison Map of the Retrieved Temperature at Specific Pressure Levels (a)200hPa; (b)500hPa; (c)600Pa; (d)700hPa; (e)850hPa; (f)1000hPa

https://doi.org/10.5194/egusphere-2025-680
Preprint. Discussion started: 17 March 2025

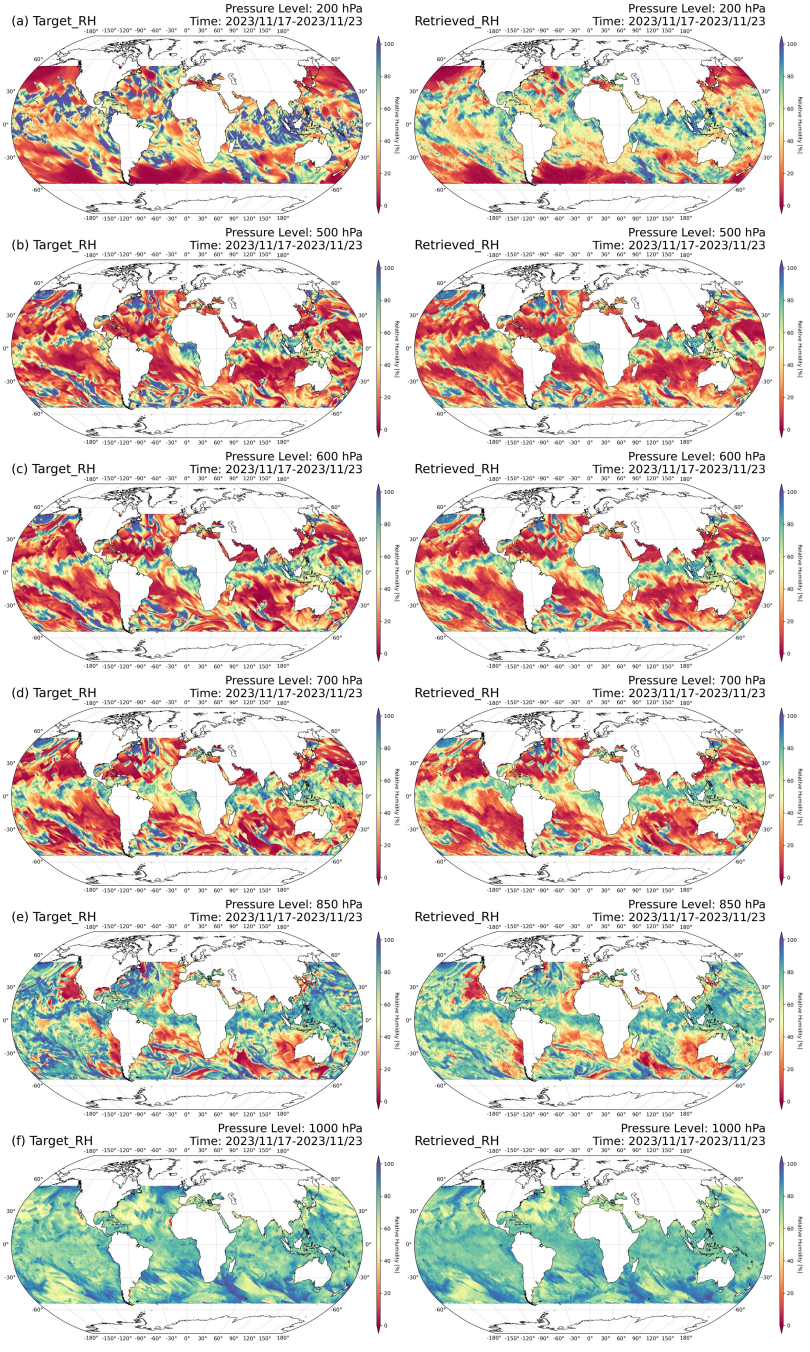

Fig. A2: Global Comparison Map of the Retrieved Relative Humidity at Specific Pressure Levels (a)200hPa; (b)500hPa; (c)600Pa; (d)700hPa; (e)850hPa; (f)1000hPa

https://doi.org/10.5194/egusphere-2025-680
Preprint. Discussion started: 17 March 2025

Author contributions. In this research, each author played a vital role. WH and ML designed the experiments, setting up the framework, procedures, and variables. ML carried out all experiments, handling equipment and data accurately. HS optimized the experimental code for better efficiency. RY verified the results through rigorous analysis. YY revised and edited the manuscript to meet the journal's high standards. Their combined efforts led to the success of this research.

Data availability. The ERA5 data are from the Copernicus Climate Change Service (C3S) Climate Data Store (CDS) (https://doi.org/10.24381/cds.bd0915c6, Hersbach et al., 2023). The training datasets used for this study can be requested from the authors.

Competing interests. The contact author has declared that none of the authors has any competing interests.

Acknowledgments. This research was supported by many individuals. We gratefully acknowledge the faculty and senior researchers at the CMA Earth System Modeling and Prediction Centre, especially Bowen Cai for satellite data remapping and Shuting Zhou for RTTOV simulations. We also thank Professors Hao Li and Xiuyu Sun from the Shanghai Academy of AI for Science for guidance on algorithm optimization and model application, which advanced our work in intelligent science and meteorological forecasting. Finally, we are grateful to all mentors who supported this research and its completion.

Financial support. This work was supported by the National Natural Science Foundation of China under Grants（U2442219 and 42205158 ）

https://doi.org/10.5194/egusphere-2025-680
Preprint. Discussion started: 17 March 2025

Reference

Aires, F., Boucher, E., and Pellet, V.: Convolutional neural networks for satellite remote sensing at coarse resolution. Application for the SST retrieval using IASI, Remote Sens. Environ., 263, 112553, https://doi.org/10.1016/j.rse.2021.112553, 2021.

Blackwell, W. J.: A neural-network technique for the retrieval of atmospheric temperature and moisture profiles from high spectral resolution sounding data, IEEE Trans. Geosci. Remote Sens., 43, 2535–2546, https://doi.org/10.1109/tgrs.2005.855071, 2005.

Burns, B. A., Wu, X., and Diak, G. R.: Model-derived brightness temperature in AMSU moisture channels for various precipitation structures: Comparison of two radiative transfer formulations, in: 1995 International Geoscience and Remote Sensing Symposium, IGARSS '95: Quantitative Remote Sensing for Science and Applications, vol. 2, Firenze, Italy, 876–878, https://doi.org/10.1109/IGARSS.1995.521084, 1995.

Burns, B. A., Wu, X., and Diak, G. R.: Effects of precipitation and cloud ice on brightness temperatures in AMSU moisture channels, IEEE Trans. Geosci. Remote Sens., 35, 1429–1437, https://doi.org/10.1109/36.649797, 1997.

Cabrera-Mercader, C. R., and Staelin, D. H.: Passive microwave humidity profile retrievals using neural networks, in: Proceedings of IGARSS '94 – 1994 IEEE International Geoscience and Remote Sensing Symposium, vol. 4, Pasadena, CA, USA, 2057–2059, https://doi.org/10.1109/IGARSS.1994.399653, 1994.

Cadeddu, M. P., Turner, D. D., and Liljegren, J. C.: A Neural Network for Real-Time Retrievals of PWV and LWP From Arctic Millimeter-Wave Ground-Based Observations, IEEE Trans. Geosci. Remote Sens., 47, 1887–1900, https://doi.org/10.1109/tgrs.2009.2013205, 2009.

Cai, X., Bao, Y., Petropoulos, G. P., Lu, F., Lu, Q., Zhu, L., and Wu, Y.: Temperature and Humidity Profile Retrieval from FY4-GIIRS Hyperspectral Data Using Artificial Neural Networks, Remote Sens., 12, 1872, https://doi.org/10.3390/rs12111872, 2020.

Cao, X. F., Li, X. Y., Luo, Q., Liu, S. H., Li, P., and Liu, X.: Review of temperature profile inversion of satellite-borne infrared hyperspectral sensors, Natl. Remote Sens. Bull., 25, 577–598, https://doi.org/10.11834/jrs.20210009, 2021.

https://doi.org/10.5194/egusphere-2025-680
Preprint. Discussion started: 17 March 2025

Chen, K., Cai, B., Han, W., and Suo, Z.: Matching of Observation Footprints in the FY-3G MWRI-RM Using BGI, IEEE J. Sel. Top. Appl. Earth Obs. Remote Sens., 17, 1–12, https://doi.org/10.1109/JSTARS.2024.3468437, 2024.

Chen, H., and Lin, L.: Numerical simulation of temperature profile retrievals from the brightness temperatures in 6 channels near 118.75 GHz, Chin. J. Atmos. Sci., 27, 894–900, https://doi.org/10.3878/j.issn.1006-9895.2003.05.10, 2003.

Ebell, K., Orlandi, E., Hünerbein, A., Löhnert, U., and Crewell, S.: Combining ground-based with satellite-based measurements in the atmospheric state retrieval: Assessment of the information content, J. Geophys. Res.-Atmos., 118, 6940–6956, https://doi.org/10.1002/jgrd.50548, 2013.

Elfwing, S., Uchibe, E., and Doya, K.: Sigmoid-weighted linear units for neural network function approximation in reinforcement learning, Neural Netw., 108, 319–331, https://doi.org/10.1016/j.neunet.2017.12.012, 2018.

Gasiewski, A. J., and Staelin, D. H.: Statistical precipitation cell parameter estimation using passive 118-GHz O2 observations, J. Geophys. Res., 94, 18367–18378, https://doi.org/10.1029/JD094iD15p18367, 1989.

Gasiewski, A. J., and Johnson, J. T.: Statistical temperature profile retrievals in clear-air using passive 118-GHz O_2 observations, IEEE Trans. Geosci. Remote Sens., 31, 106–115, https://doi.org/10.1109/36.210450, 1993.

Guan, L., Liu, Y., and Zhang, X.-H.: Application of artificial neural network algorithm in retrieving atmospheric temperature profile from infrared hyperspectral data, J. Atmos. Sci., 33, 341–346, 2010.

Gu, S., Zhang, P., Chen, L., Shang, J., Zhang, H., Lin, M., Zhu, A., Jia, S., Yin, H., Sun, F., Xu, H., Wang, H., Li, L., Wu, Q., Guo, Y., Dou, F., and Wu, S.: Overview and prospect of the detection capability of China's first precipitation measurement satellite FY-3G, Torrential Rain Disasters, 42, 489–498, https://doi.org/10.12406/byzh.2023-106, 2023.

He, K., Zhang, X., Ren, S., and Sun, J.: Deep residual learning for image recognition, in: 2016 IEEE Conference on Computer Vision and Pattern Recognition (CVPR), Las Vegas, NV, USA, 770–778, https://doi.org/10.1109/CVPR.2016.90, 2016.

https://doi.org/10.5194/egusphere-2025-680
Preprint. Discussion started: 17 March 2025

He, Q. R., Wang, Z. Z., and He, J. Y.: Retrieval of clear sky temperature and humidity profiles over land using measurements of FY-3C/MWHTS, J. Remote Sens., 21, 27–39, https://doi.org/10.11834/jrs.20176006, 2017.

Hersbach, H., Bell, B., Berrisford, P., et al.: ERA5 hourly data on pressure levels from 1940 to present, Copernicus Climate Change Service (C3S) Climate Data Store (CDS), 2023, https://doi.org/10.24381/cds.bd0915c6.

Ioffe, S. and Szegedy, C.: Batch Normalization: Accelerating Deep Network Training by Reducing Internal Covariate Shift, arXiv preprint, arXiv:1502.03167, 2015.

King, J. I.: The Radiative Heat Transfer of Planet Earth, 1958.

Liu, Y., Mao, J., Liu, J., and Li, F.: Study on BP neural network retrieval method of atmospheric profile using ground-based microwave radiometer, Plateau Meteorology, 29, 1514–1523, 2010.

Malmgren-Hansen, D., Laparra, V., Nielsen, A. A., and Camps-Valls, G.: Statistical retrieval of atmospheric profiles with deep convolutional neural networks, ISPRS J. Photogramm. Remote Sens., 158, 231–240, 2019, https://doi.org/10.1016/j.isprsjprs.2019.10.002.

Rosenkranz, P. W.: Retrieval of temperature and moisture profiles from AMSU-A and AMSU-B measurements, IEEE Trans. Geosci. Remote Sens., 39, 2429–2435, 2001, https://doi.org/10.1109/36.964979.

Sahoo, S., Bosch-Lluis, X., Reising, S. C., and Vivekanandan, J.: Radiometric Information Content for Water Vapor and Temperature Profiling in Clear Skies Between 10 and 200 GHz, IEEE J. Sel. Top. Appl. Earth Obs. Remote Sens., 8, 859–871, 2015, https://doi.org/10.1109/JSTARS.2014.2364394.

Smith, W. L.: Iterative solution of the radiative transfer equation for the temperature and absorbing gas profile of an atmosphere, Appl. Opt., 9, 1993–1999, 1970.

Smith, W. L. and Woolf, H. M.: The use of eigenvectors of statistical covariance matrices for interpreting satellite sounding radiometer observations, J. Atmos. Sci., 33, 1127–1140, 1976.

Solheim, F., Godwin, J. R., Westwater, E. R., Han, Y., Keihm, S. J., Marsh, K., and Ware, R.: Radiometric profiling of temperature, water vapor and cloud liquid water using various inversion methods, Radio Sci., 33, 393–404, 1998, https://doi.org/10.1029/97RS03656.

https://doi.org/10.5194/egusphere-2025-680
Preprint. Discussion started: 17 March 2025

Susskind, J., Barnet, C. D., and Blaisdell, J. M.: Retrieval of atmospheric and surface parameters from AIRS/AMSU/HSB data in the presence of clouds, IEEE Trans. Geosci. Remote Sens., 41, 390–409, 2003, https://doi.org/10.1109/TGRS.2002.808236.

Tan, Q., Yao, Z., Zhao, Z., Han, Z., and Sun, X.: Performance analysis of atmospheric temperature and humidity profile retrieval using multiband microwave radiometer, Remote Sens. Technol. Appl., 30, 170–177, 2015.

Wang, D., Tong, L., Gong, X., Guan, X., Wang, P., and Gao, B.: Retrieval of atmospheric temperature profiles from hyperspectral microwave radiative data based on the neural network, in: Proceedings of the IEEE International Geoscience and Remote Sensing Symposium (IGARSS), Brussels, Belgium, 7095–7098, https://doi.org/10.1109/IGARSS47720.2021.9554282, 2021.

Wang, H., Liu, D., Xia, Y., Xie, W., and Wang, Y.: Retrieval of atmospheric temperature profile from historical data and ground-based observations by using a machine learning algorithm, Remote Sens., 15, 2717, https://doi.org/10.3390/rs15112717, 2023.

Wang, X., Song, G., Yao, Z., and Li, W.: Study on the retrieval of atmospheric humidity profiles over the northwestern Pacific Ocean using AMSU data, J. Peking Univ. (Nat. Sci. Ed.), 46, 69–78, https://doi.org/10.13209/j.0479-8023.2010.011, 2010.

Weinman, J. A.: The effect of cirrus clouds on 118-GHz brightness temperatures, J. Geophys. Res., 93, 11059–11062, https://doi.org/10.1029/JD093iD09p11059, 1988.

Wu, X., Li, J., Zhang, W., and Wang, F.: Atmospheric profile retrieval with AIRS data and validation at the ARM CART site, Adv. Atmos. Sci., 22, 647–654, https://doi.org/10.1007/BF02918708, 2005.

Xu, X., Han, W., Gao, Z., Li, J., and Yin, R.: Retrieval of atmospheric temperature profiles from FY-4A/GIIRS hyperspectral data based on TPE-MLP: analysis of retrieval accuracy and influencing factors, Remote Sens., 16, 1976, https://doi.org/10.3390/rs16111976, 2024.

Yao, S. H., and Guan, L.: Retrieval of atmospheric temperature and humidity profiles using a machine learning algorithm based on satellite-borne infrared hyperspectral observations, Infrared Laser Eng., 51, 461–472, 2022.

Zhang, C., et al.: A study on the retrieval of temperature and humidity profiles based on FY-3D/HIRAS infrared hyperspectral data, Remote Sens., 13, 2157, https://doi.org/10.3390/rs13112157, 2021.

https://doi.org/10.5194/egusphere-2025-680
Preprint. Discussion started: 17 March 2025

Zhang, J., Liu, P., Zhang, F., and Song, Q.: CloudNet: ground-based cloud classification with deep convolutional neural network, Geophys. Res. Lett., 45, 8665–8672, https://doi.org/10.1029/2018GL077787, 2018.

Zhang, P., Gu, S., Shang, J., Zhang, H., Chen, L., Lin, M., Zhu, A., Jia, S., Wu, S., and Xian, D.: Overview of the mission of China's first precipitation satellite—FY-3G, Int. Space, 6, 17–21, 2023.

Zhu, X., Yee, J., and Talaat, E. R.: Diagnosis of dynamics and energy balance in the mesosphere and lower thermosphere, J. Atmos. Sci., 58, 2441–2454, https://doi.org/10.1175/1520-0469(2001)058<2441:DODAEB>2.0.CO;2, 2001.